Whole slide imaging is a high-throughput method to assess *Candida* biofilm formation

Maximilian W. D. Raas [1,2], Thiago P. Silva[1], Jhamine C. O. Freitas[3], Lara M. Campos[3], Rodrigo L. Fabri[3], Rossana C.N. Melo[1*]

[1]Laboratory of Cellular Biology, Department of Biology, ICB, Federal University of Juiz de Fora, UFJF, Juiz de Fora, MG, Brazil.

[2]Faculty of Medical Sciences, Radboud University, Geert Grooteplein 10, Nijmegen, The Netherlands

[3]Bioactive Natural Products Laboratory, Department of Biochemistry, Institute of Biological Sciences, Federal University of Juiz de Fora, UFJF, Juiz de Fora, MG, Brazil.

*** Correspondence:** rossana.melo@ufjf.edu.br

Short title: **WSI applied to *Candida* biofilms**

Keywords: *Candida spp*., digital microscopy, virtual microscopy, antifungal agents, biofilms, scanning electron microscopy, whole slide imaging.

Abstract

New strategies that enable fast and accurate visualization of *Candida* biofilms are necessary to better study their structure and response to antifungals agents. Here, we applied whole slide imaging (WSI) to study biofilm formation of *Candida* species. Three relevant biofilm-forming *Candida* species (*C. albicans* ATCC 10231*, C. glabrata* ATCC 2001*,* and *C. tropicalis* ATCC 750) were cultivated on glass coverslips both in presence and absence of widely used antifungals. Accumulated biofilms were stained with fluorescent markers and scanned in both bright-field and fluorescence modes using a WSI digital scanner. WSI enabled clear assessment of both size and structural features of *Candida* biofilms. Quantitative analyses readily detected reductions in biofilm-covered surface area upon antifungal exposure. Furthermore, we show that the overall biofilm growth can be adequately assessed across both bright-field and fluorescence modes. At the single-cell level, WSI proved adequate, as morphometric parameters evaluated with WSI did not differ significantly from those obtained with scanning electron microscopy, considered as golden standard at single-cell resolution. Thus, WSI allows for reliable visualization of *Candida* biofilms enabling both large-scale growth assessment and morphometric characterization of single-cell features, making it an important addition to the available microscopic toolset to image and analyze fungal biofilm growth.

INTRODUCTION

Biofilms are defined as surface-attached, highly resistant, multicellular microbial communities. They are the product of numerous microbes aggregating and some organisms have been observed to wholly merge in this process (Douglas, 2003; Hall-Stoodley, et al., 2004). The main constituents of these remarkably resilient structures when produced by yeast-type fungal species are filamentous hyphae, pseudohyphae, yeast-form cells and a self-produced heterogeneous extracellular matrix (Fanning & Mitchell, 2012; Lagree, et al., 2018).

Candida biofilm resilience encompasses several aspects. Firstly, they are highly resistant to antifungal agents. Furthermore, when compared to planktonic phase fungal cells, biofilm infections have increased virulence, higher recurrence rates and are known to readily disperse, forming secondary infection sites (Del Pozo, 2018; Nobile & Johnson, 2015; Ramage, et al., 2012; Uppuluri, et al., 2010). In addition, these pathogenic structures have been shown to suppress immune responses, rendering the host's intrinsic defences ineffective (Kernien, et al., 2017; Xie, et al., 2012). Taken together, *Candida* biofilms are hard to eradicate and actively promote their survival, procreation and virulence.

As fungal infection disease burden rises alongside increasingly prevailing resistance, research into the fungal biofilm architecture and their response to antifungal agents is becoming more and more pivotal towards successful treatment strategies. A widely used methodology in this research field is scanning electron microscopy (SEM). It provides detailed, ultra-high spatial resolution of the complex three-dimensional (3D) structure that is a biofilm. Other traditional microscopy techniques have been used as well, such as conventional light microscopy and confocal laser scanning microscopy (Lagree, et al., 2018), mainly to study local architecture and molecular markers, respectively (Paulitsch, et al., 2009). Using these techniques, many meaningful insights concerning architecture and mechanisms of resistance have been acquired.

However, traditional microscopy methods are time-consuming and have their limitations when it comes to complete evaluation of large-scale architecture and biofilm response to antifungal agents, as these techniques focus on a very small section of a biofilm from which the whole structure has to be estimated (Azeredo, et al., 2017). Since biofilms are highly complex, multifaceted and heterogeneous (Kean, et al., 2018; Wimpenny, et al., 2000), this limited view will oftentimes lead to interpretative flaws in understanding the complete structure.

In order to obtain more insights into the cohesion of domains inside a biofilm and to investigate whole biofilm architecture normally growing or following exposure to antifungals, we address here the use of a technique new to the field of biofilm research: whole slide imaging (WSI). This approach allows high-resolution, digital visualization of regular glass slides in their entirety with the use of a digital slide scanner thus generating "digital slides" that offer detailed morphological information and possibility for quantification of multiple morphometric parameters (Amaral, et al., 2017; Melo, et al., 2019; Webster & Dunstan, 2014). Other WSI benefits are digital storage, easy share ability, the possibility to make annotations on the slide, automated data extraction, remote accessibility and educational purposes (Saco, et al., 2016).

In the present work, WSI was applied, for the first time, to compare biofilm formation of three species of *Candida* (*C. albicans, C. glabrata,* and *C. tropicalis*) normally growing in cultures and after treatment with antifungals. Our findings demonstrate that WSI is a powerful tool to assess *Candida* biofilm extent and is able to reveal biofilm morphology even at single-cell level.

106

107

108 **MATERIALS & METHODS**

109 **Fungal strains**

110 The following yeast strains were used in this study: *Candida albicans* ATCC® 10231™,
111 *Candida glabrata* ATCC® 2001™ and *Candida tropicalis* ATCC® 750™. These strains were
112 cultured at 35ºC for 24h (*C. albicans* and *C. glabrata*) or 48h (*C. tropicalis*) in Sabouraud
113 dextrose agar (SDA) before all experiments (Campos, et al., 2018).

114

115 **Minimal inhibitory concentration (MIC)**

116 The MIC of fluconazole or nystatin was determined by serial microdilution technique
117 according to CLSI-M27 (Rex, 2008). The stock solution of antifungals (fluconazole or nystatin) was
118 diluted in dimethylsulfoxide (DMSO - final concentration of 1%) to obtain concentrations ranging
119 from 100 to 0.78 µg/mL (*C. glabrata* and *C. tropicalis*) or 1,000 to 7.8 µg/mL (*C. albicans*). All
120 tests were performed in a volume of 200 µL and plates were incubated at 35ºC for 24h (*C. albicans*
121 and *C. glabrata*) or 48h (*C. tropicalis*) . Controls were established without the addition of any
122 antifungal. The MIC values were calculated as the highest dilution showing complete inhibition of
123 tested strain. All analyses were performed in triplicate.

124

125 **Biofilm cultures and antimicrobial treatment**

126 Fungal strains were seeded in Sabouraud Dextrose Agar (SDA), incubated (35°C, *C. albicans*
127 *and C. glabrata:* 24h, C. tropicalis: 48h), and inoculated into a tube with 5 mL of Sabouraud
128 Dextrose Broth (SDB) supplemented with glucose (Aggarwal & Kashyap, 2018; Paiva, et al., 2012).
129 Then, 500 µL of the inoculated broth were added in microtiter plates (24 wells) containing high-
130 adhesion round German glass coverslips (Catalog # 72296-08, EMS, Hatfield, PA, USA), which are
131 used for growing and culturing cells that normally have poor adhesion to regular glass surfaces. For
132 each strain, treatment was performed by adding 500 µL of fluconazole (n=4) or nystatin (n=4) at 1
133 MIC final concentration per well. Wells without addition of any antifungal served as growth controls
134 (n = 4 for each strain). Sterile controls were done in wells with broth only. *C. albicans* and *C.*
135 *glabrata* microtiter plates were incubated for 24h at 35°C and *C. tropicalis* plates were incubated for
136 48h at 35°C.

137

138 **Biofilm staining**

139 Two classical fluorescent dyes were used for yeast detection, 4′,6-Diamidine-2′-phenylindole
140 dihydrochloride (DAPI) and Calcofluor White (CW). DAPI is a fluorescent dye that binds
141 selectively to double-stranded DNA and CW is a non-specific fluorophore that binds to cellulose and
142 chitin found in cell walls (Hageage & Harrington, 1984; Kapuscinski, 1995). After incubation,

143 supernatants were removed from wells and coverslips were gently washed with sterile phosphate-
144 buffered saline (0,1 M, pH 7,4 PBS) to remove nonadherent cells. Then, biofilms on coverslips (n=
145 48, 12 for each strain) were fixed in freshly prepared formaldehyde solution (final concentration
146 3.7% in 0,1 M, pH 7,4 PBS) for 30 min. Then, the fixative solution was removed and the coverslips
147 were gently washed with sterile distilled water. Biofilm staining was done by covering the coverslips
148 with 10 µL of DAPI (0.01 µg/mL in PBS, Sigma-Aldrich, USA) or CW stain solution (CW M2R
149 [0.001 g/mL] and evans blue [0.0005 g/mL], Sigma-Aldrich, USA) for 5-10 min in the dark. All
150 steps of fixation and staining were done directly in microtiter plate wells. Next, each coverslip was
151 carefully removed from the plates and attached (side opposite to biofilm) on the surface of a regular
152 glass slide using Entellan mounting medium (Merck, Darmstadt, Germany) for subsequent scanning
153 as below.

154

155 **Image acquisition**

156 A WSI scanner is a robotic microscope capable of digitizing an entire glass slide, using
157 software to merge or stitch individually captured images into a composite digital image (Webster &
158 Dunstan, 2014). The images generated through this technology are commonly referred to as whole
159 slide images, WSIs, whole slide scans or digital slides (Farahani, et al., 2015). DAPI and CW stained
160 coverslips from the three *Candida* species were digitally scanned in two different modalities
161 (fluorescence and bright-field) using a 3D Scan Pannoramic Histech scanner (3D HistechKft,
162 Budapest, Hungary) connected to a computer (Fujitsu Technology Solutions GmbH, Munich,
163 Germany). High-resolution images (tiff files uncompressed RGB with 300 DPI) obtained from slides
164 scanned at fluorescence (DAPI and CW) and bright-field modes were acquired using Pannoramic
165 Viewer 1.15.2 SP2 RTM software (3D Histechkft Budapest, Hungary) at different digital
166 magnifications (1-100 X).

167

168 **Image processing and total biofilm area**

169 Image processing and morphometric analyses of *Candida* biofilms were done using *FIJI*
170 software (National Institutes of Health, Bethesda, MD). First, digital images from CW and DAPI-
171 stained biofilms, scanned at both fluorescent and bright-field modes, were acquired from the entire
172 surface of the glass coverslips at 1- 4x digital magnification and converted to binary (black and
173 white, 0-255) images. Next, images were thresholded to highlight just the biofilm areas through pixel
174 saturation. The threshold processing was done in comparison to the original images to ensure the
175 accuracy of all biofilm areas. Then, quantification of the coverslip areas covered by biofilms was
176 performed by measuring the saturated-pixel areas and establishing the proportions of biofilms.

177

178 **Scanning electron microscopy**

179 *C. albicans*, *C. glabrata* and *C. tropicalis* biofilms (fluconazole and nystatin-treated and
180 respective controls) on the surface of coverslips were fixed in freshly prepared aldehydes (1%
181 paraformaldehyde and 1.25% glutaraldehyde) in 0.1 M, pH 7.4 phosphate buffer for 1 h at room
182 temperature and processed as before (Lemos, et al., 2018). After post-fixation in 1% osmium
183 tetroxide, the biofilms were washed in phosphate buffer and dehydrated through a graded series of
184 ethanol solutions (30%, 50%, 70%, 90% and twice in 100%) for 15 min at each concentration. Then,

185 samples were critical point dried in carbon dioxide. Subsequently, coverslips were mounted on
186 aluminium holders, sputtered with 5 nm gold and imaged with a double beam scanning electron
187 microscope (Quanta™ 3D FEG, FEI Company, Hillsboro, OR, USA). To study the ultrastructural
188 aspects of the cells, electron micrographs were taken at magnifications of 2,000 – 25,000×.

189

190 **Cell morphology analyses**

191 The assessment of *Candida* cellular morphology in biofilms was done by both WSI (cells
192 stained with CW) and SEM. Scanned images (40-100× digital magnification, RGB or grayscale)
193 from CW stained biofilms and electron micrographs (magnifications of 5,000-25,000×) were
194 analyzed using FIJI software (National Institutes of Health, Bethesda, MD). Cell area and roundness
195 were analyzed for a total of 680 yeast cells as shown in Table 1. The roundness was automatically
196 calculated by 4*area/(π*major_axis^2), with 1.0 indicating a perfect circle and larger values
197 indicating oblong cells.
198
199 Table 1: Number of *C. albicans*, *C. glabrata* and *C. tropicalis* cells analyzed by WSI and SEM.

Experimental Groups	*C. albicans*		*C. glabrata*		*C. tropicalis*	
	WSI	SEM	WSI	SEM	WSI	SEM
Growth control (GC)	41	50	46	40	34	33
Fluconazole	40	50	36	40	21	35
Nystatin	34	44	41	28	39	28
Total (n)	**115**	**144**	**123**	**108**	**94**	**96**

200

201 **Statistical Analysis**

202 Data from biofilm areas and cell morphology were compared using Anova followed by
203 Tukey's comparison test, or Kruskal-Wallis test. The relationship between biofilm areas acquired by
204 different scan modalities (bright-field and fluorescence [DAPI or CW]) was determined using least
205 square regression. All statistics was performed using GraphPad Prism version 8.00 for Windows
206 (GraphPad Software, La Jolla California, www.graphpad.com), considering $P < 0.05$ as a threshold
207 level for significance.

208

209

210 **RESULTS**

211 **MIC analyses**

212 The MIC assay indicates susceptibility or resistance of fungal strains. First, we evaluated the
213 MIC for all fungal strains in response to fluconazole or nystatin as presented in Table 2.

214

215

216 Table 2: MIC values for fluconazole and nystatin for the different fungal strains

Candida species	MIC Fluconazole (μg/mL)	MIC Nystatin (μg/mL)
C. albicans	1,000	2.5
C. glabrata	50	12.5
C. tropicalis	12.5	12.5

217 Strains are considered susceptible to fluconazole if their MIC is <64 μg/mL. Subsequently,
218 resistance is defined at having a MIC of ≥64 μg/mL (Ghannoum & Rice, 1999; Pfaller, et al., 2006).
219 For nystatin, the breakpoint is defined as a MIC of <16 μg/mL (=susceptibility) and ≥16 μg/mL
220 (=resistance) (Kuriyama, et al., 2005). Given this information, *C. albicans* strain can be considered
221 resistant to fluconazole and susceptible to nystatin. The other strains (*C. glabrata* and *C. tropicalis)*
222 were considered susceptible to both fluconazole and nystatin.

223

224 **Assessment of biofilms with WSI**

225 Having established the MICs for all strains, cultures of *Candida* species were grown on the
226 surface of round glass coverslips within plates with or without the presence of antifungal agents (Fig.
227 1). After the incubation period, coverslips were stained with two different fluorophores [DAPI
228 (n=24) and CW (n=24)], affixed on glass slides and scanned in a digital scanner with three different
229 WSI strategies: bright-field (BF) mode (all slides, n=48), fluorescence mode after DAPI staining
230 (n=24) and fluorescence mode after CW staining (n=24) (Figs 1A-D). Thus, a total of 96 high-
231 resolution virtual images covering the total biofilm area were acquired for subsequent viewing and
232 morphometric analyses using software (Figs 1E, F). Each virtual image represents an entire glass
233 coverslip/slide (Fig. 1). Comparisons were drawn between BF and fluorescence modalities to explore
234 their accuracy and reliability.

235

236 **WSI enables reliable quantification of biofilm development**

237 The biofilm surface area is a reliable measure of the fungal ability to attach to a surface and
238 proliferate (Rex, 2008). Here, we used coverslips made with German glass, which provide high
239 adhesion of cells in cultures and are indicated for optimal imaging with fluorescent probes, to
240 successfully grow Candida biofilms and then applied WSI. In growth control samples, we clearly
241 notice the formation of consistent biofilms attached on the surface of coverslips (Figs 2 A-C).
242 Considering all scan strategies together (bright field and fluorescence), our quantitative analyses
243 showed that GC biofilms covered more than 80% of the coverslips surface (Figs 2 D-F). Thus, WSI
244 showed to be a very useful tool to examine large-scale biofilms of *Candida* species, both in normal
245 growth and in the presence of antifungal agents, as shown below for each species.

246

247 *C. albicans*

248 Compared to the control group (Figs 2A, Ai), fluconazole exposure did not affect biofilm
249 formation and adhesion of the fluconazole-resistant *C. albicans* across the coverslips (Fig. 3 A). On
250 the other hand, nystatin-exposed *C. albicans* cells were not able to establish any meaningful biofilm

251 on the coverslip (Figs 3 A, D). WSI quantitative analyses in all WSI modalities showed a significant
252 decrease of biofilm-covered area in the presence of antifungals (. 3F; $P<0.0001$ for all). When the
253 extent of biofilms acquired with different WSI modalities were compared, there were no significant
254 differences among all three strategies (Fig. 3F; $P>0.999$ for all).
255
256 *C. glabrata*

257 This *Candida* strain was susceptible to both antifungals. This was clearly demonstrated by the
258 extent of formed biofilms. While in the control group (Figs 2A, Ai), biofilms occupied most of the
259 coverslip surface, treated samples displayed very low levels of biofilm coverage (Figs 3B, E).
260 Measurements of the biofilm-covered areas taken in all scanning modalities confirmed the drastic
261 decrease in the amount of biofilm formed following exposure to antifungals compared to the control
262 group (Fig. 3G; $P<0.0001$). As shown for *C. albicans*, individual WSI modes did not affect
263 visualization of biofilm areas (Fig. 3G; $P>0.999$ for all). In each WSI modality, a significant decrease
264 in the proportion of biofilm coverage was observed after fluconazole or nystatin treatments (BF,
265 DAPI, CW: $P<0.0001$ for each).

266
267 *C. tropicalis*
268 This *Candida* strain showed no resistance during the MIC experiments. Accordingly,
269 compared to the control group (Figs 2A, Ai), large decreases in the biofilm extent were observed by
270 *C. tropicalis* in the presence of fluconazole or nystatin (Fig. 3C, F; $P<0.0001$). Quantitative analyses
271 in all WSI modes confirmed a significant reduction in the proportion of biofilm-covered areas after
272 both treatments in comparison to the control group (Fig. 3H; $P<0.0001$). Each individual WSI mode
273 also detected significant reduction of the biofilm areas in response to antifungals (BF, DAPI, CW:
274 $P<0.0001$).

275 Of note, application of an additional statistical method (regression analysis) for all *Candida*
276 species and treatments demonstrated that the total surface area of biofilms measured under different
277 WSI modalities were correlated thus demonstrating that the biofilm areas can be reliably detected by
278 BF and fluorescence modes (Fig. S1).

279

280 **WSI is a useful tool to assess biofilm structure**

281 By measuring the biofilm areas visualized with WSI, we noticed that additional information
282 on structural aspects of *Candida* biofilms could be obtained from the high-resolution images when
283 seen in high magnification. Thus, WSI revealed the organization of the biofilms for the different
284 *Candida* species (Fig. 4). *C. albicans* generally clustered in one large and highly dense biofilm with
285 channel-like structures flowing through them (Figs 4A, B). This aspect was not seen for *C. glabrata*
286 (Figs 4C, D) *and C. tropicalis* (Fis. 4E, F) biofilms, which appeared as a less dense structure with
287 typical meshwork aspect. While *C. glabrata* biofilm is characterized by thin filamentous stretches of
288 relatively small fungal cells surrounding an empty, almost round opening (Figs 4C, D), *C. tropicalis*
289 (Figs 4E, F) forms a meshwork with thicker septa with a slightly lesser cell density. These septa also
290 include circular openings of their own creating an intricate pattern presented.

291 WSI also showed the presence of filamentous cells (hyphal forms) in biofilms of all *Candida*
292 species (Figs 5A-C), indicative of vegetative growth through a filamentation process, which is
293 considered a virulence factor (Berman, 2006). Hyphal forms are frequently present in the later latter

294 stages of fungal biofilms maturation and can represent pseudohyphae or true hyphae in *Candida*
295 biofilms (Roilides & Ramage, 2017). Division and constriction septa between cells in the filament
296 were clearly observed when the samples were stained with CW (Fig. 5A).

297

298 **WSI reveals biofilm morphology at single-cell level**

299 WSI revealed not only the species-specific organization of the biofilms (Fig. 4), but also
300 morphological aspects (cell shape) of individual yeast cells. High-resolution WSI analyses of
301 biofilms stained with CW, which enables visualization of the cell surface (cell wall), enabled the
302 observation of round and elongated yeasts cells in both RGB (Figs 6A-C) and grayscale (Figs 6D-F).

303 To evaluate the accuracy of biofilm-composed yeast cell shapes, we next prepared additional
304 samples of *Candida* species growing in normal conditions to SEM, a technique considered to be the
305 "gold standard" to study cell morphology in biofilms (Azeredo, et al., 2017). SEM (Figs 6G-I)
306 showed in 3D the same morphological aspects depicted by WSI images (Fig. 6A-F). We then applied
307 quantitative analyses to evaluate cell area and cell roundness in the images acquired by both WSI and
308 SEM. These two parameters are considered relevant to study yeast cell shapes (Bougen-Zhukov, et
309 al., 2017; Lee, et al., 2011; Liu, et al., 2011; Wang & Lin, 2012). In all cases, the data for cell
310 morphometric assessment with WSI did not differ from the data acquired with SEM (P >0.90 for all),
311 indicating that the resolution of WSI is accurate at this level and for this purpose.

312 Remarkably, morphometric analyses revealed that the area of individual yeast cells in the
313 biofilm significantly varies depending on the *Candida* species and that this variation can be detected
314 by both WSI and SEM (Figs 6J, $P < 0.0001$). Cell roundness analyses, done with both WSI and SEM
315 images, revealed significant differences when *C. albicans* was compared to *C. glabrata* (Fig. 7K, $P =$
316 0.01). Additionally, cell budding was clearly identified by both WSI (Figs 6L, M) and SEM (Figs
317 6N, O) in all three species in process of vegetative growth. Both WSI and SEM revealed that while
318 mother cells exhibited a more elongated shape, budding cells had a pronounced round shape and
319 smaller size (Figs 6L-N). "Bud Scars" on the surface of some yeast cells were seen in detail by SEM
320 (Figs 6O and 6Oi). Evidence of budding was more frequently observed in *C. glabrata*, which could
321 explain their reduced area and roundness in comparison with *C. albicans* and *C. tropicalis* (Figs 6J
322 and 6K).

323

324 **DISCUSSION**

325 Most fungal pathogens exist as adhered cells to surfaces within a well-organized biofilm
326 ecosystem and not as free-floating organisms. However, the architecture of fungal biofilms is not
327 fully understood. In the present study, we explore the use of WSI as an approach for large-scale
328 imaging of *Candida* biofilms. One of the advantages of WSI is that it produces images with high
329 resolution and, at the same time, with a wide field of observation. Here, we show that *Candida*
330 species were able to attach and grow as biofilms on coverslips, as expected (Malm, et al., 2010;
331 Silva-Dias, et al., 2015) and that WSI application facilitated comprehensive visualization of *Candida*
332 biofilms both in natural growth and in presence of antifungal agents. Moreover, WSI combined with
333 computational methods enabled fast quantification of the adhesion extent of *Candida* biofilms. Thus,
334 WSI showed to be a very useful tool to examine large-scale biofilms of *Candida* species, since in
335 growth control samples biofilms covered most surfaces of the coverslips.

Our data show that inhibitory concentrations of antifungal agents applied to planktonic fungi can effectively inhibit the formation of biofilms. However, MIC concentration applied to a *C. albican*s resistant-strain did not led to significant decreases in the amount of biofilm formed by this strain within a 24h period as expected. Both biofilm formation and biofilm reduction after treatment with antifungals were properly detected by WSI. Our findings demonstrated no variation in the reduction of area covered by biofilms after treatments when WSI modalities were compared. Thus, WSI can be a valuable tool to accurately test biofilm responses to antifungals regardless if the images are acquired under bright-field or fluorescence (DAPI and CW) WSI modes, indicating reliability of WSI settings.

Remarkably, not only the extent but also structural aspects of biofilms were captured by WSI. This approach revealed, for example, that *C. albicans* form complex and highly organized channels which appear as a ramifying system of channels inside its biofilm that, to our knowledge, have been scarcely studied. As these channels are important size-determining aspects of a biofilm due to their facilitation of nutrient-flow (Ramage, et al., 2001), WSI can be particularly useful to address future studies focused on these structures. Moreover, our approach with WSI enabled detection of hyphal forms (Fig. 5) in all three *Candida* species even in the absence of a specific induction of this process. Filamentous growth, although not strictly essential for biofilm formation, provides protection and adhesion sites for the budding yeast cells and contributes to the overall robustness of the biofilm (de Barros, et al., 2020; Nobile & Johnson, 2015; Roilides & Ramage, 2017). Other structural components revealed by WSI such as division and constriction septa between cells of the filament forms are associated with pseudohyphal formation in *Candida* species (Berman, 2006).

Since WSI delivers high-resolution images, it also offers the possibility to perform high amount of analyses at the single-cell level, thus extracting more biologically significant cellular information. This has been the case of WSI applications to pathological analyses of biopsies in different fields. For example, in the field of liver pathology and biology, WSI has been extensively used for different purposes, such as to understand cellular diversity of hepatic progenitors, scoring of inflammatory cells and identification of specific hepatocarcinoma cell alterations [reviewed in (Campos, et al., 2019)].

Here, we expand the application of WSI to understand morphological aspects of *Candida* species within a biofilm. Our data showed that WSI is a reliable tool for evaluation of the cell area and ~~cell~~ roundness yeast cells as addressed by fluorescence WSI modality. Cellular area and roundness are important parameters related to environmental conditions and can even reflect specific yeast molecular features, such as cell cycle phase, genetic expression (phenotypic characteristics) or virulence (Bougen-Zhukov, et al., 2017; Lee, et al., 2011; Liu, et al., 2011; Wang & Lin, 2012). Our quantitative analyses revealed that these parameters can vary among *Candida* species (Fig. 6) and therefore WSI can be beneficial to understand cell behavior within a biofilm. Yet, the morphometric data acquired from WSI scans showed no significant differences from data extracted from SEM, a technique widely used for biofilm studies and accepted as particularly accurate at single-cell resolution (Azeredo, et al., 2017). Moreover, by observing *Candida* biofilms by WSI, we detected cell budding, which is a common division process for both haploid (*C. glabrata*) and diploid (*C. albicans* and *C. tropicalis*) yeast cells of *Candida* species (Branduardi, et al., 2012), which was confirmed by SEM.

WSI was also found to be a practical approach for imaging *Candida* biofilms. The digitalization is fully automated, and wide-field images can be stored. Complete slide scanning means that every slide can be entirely revisited at any point allowing more detailed assessment as the

analyses are not confined to limited fields-of-view captured with a regular light microscope fitted with a camera. Easy accessibility, shareability and storage allowed us to explore and quantify data from the scans using adequate software. The possibility to make annotations on slides was also very convenient, since this procedure highlights specific sections of the scan thus facilitating discussion, including remote access. On the other hand, by our experience, WSI does have some limitations for biofilm studies, especially when using unfixed biofilms stained with fluorochromes, which does not allow adequate focus. The scanning process of fluorescent samples also takes more time compared to bright-field modality, but this issue has been addressed with new generation of scanners.

Finally, our group is the first to apply WSI to understand fungal biofilms produced by different species of Candida with perspective of applications to other fungal biofilms. We recently showed that WSI is helpful to test the potential antifungal action of a phytocompound against a multidrug-resistant *C. tropicalis* strain (Lemos, et al., 2020). WSI can be also useful to study bacterial biofilms. This technique enabled to examine biofilms produced by *Salmonella enterica* strains after treatment with plant extracts with potential anti-bacterial activity (Campos, et al., 2019) and to investigate antibiotic resistance at single-bacterium level (Song, et al., 2019).

In conclusion, WSI is an emerging technique that proved to be a powerful tool in delivering an accurate, high-resolution and full-length view of *Candida* biofilms and therefore can be a worthy and efficient addition to the available microscopic toolset to image and analyse fungal biofilms.

Competing interests

The authors declare that they have no competing interests.

Funding

This work was supported in part by Conselho Nacional de Desenvolvimento Científico e Tecnológico (CNPq, Brazil), Grants 309734/2018-5 and 434914/2018-5 for RCNM and Fundação de Amparo a Pesquisa do Estado de Minas Gerais (FAPEMIG, Brazil).

Author's contributions

RM provided the study design, study mentorship and critical editing of the manuscript. MR, TS and RF contributed to the study design. MR and TS performed experiments and acquired and analyzed the data. JF and LC performed cultures. All authors contributed in part to writing and editing the manuscript and approved the final version.

Acknowledgements

The authors would like to thank Andreia Alvim for helpful discussions as well as suggestions made during the scanning electron microscopy analyses. We thank the UFMG Microscopy Center (Centro de Microscopia da UFMG, Belo Horizonte, MG, Brazil) for technical support in sample preparation and image acquisition for scanning electron microscopy.

419

420 **References**

421 AGGARWAL, P. & KASHYAP, B. (2018). Biofilm production by clinically isolated Candida:
422 Comparative analysis based on specimen, methodology, and various Candida species. Indian
423 J Med Special **9**(2), 69-72.

424 AMARAL, K.B., SILVA, T.P., DIAS, F.F., MALTA, K.K., ROSA, F.M., COSTA-NETO, S.F., GENTILE, R. &
425 MELO, R.C.N. (2017). Histological assessment of granulomas in natural and experimental
426 *Schistosoma mansoni* infections using whole slide imaging. PLoS One **12**(9), e0184696.

427 AZEREDO, J., AZEVEDO, N.F., BRIANDET, R., CERCA, N., COENYE, T., COSTA, A.R., DESVAUX, M., DI
428 BONAVENTURA, G., HEBRAUD, M., JAGLIC, Z., KACANIOVA, M., KNOCHEL, S., LOURENCO, A.,
429 MERGULHAO, F., MEYER, R.L., NYCHAS, G., SIMOES, M., TRESSE, O. & STERNBERG, C.
430 (2017). Critical review on biofilm methods. Crit Rev Microbiol **43**(3), 313-351.

431 BERMAN, J. (2006). Morphogenesis and cell cycle progression in *Candida albicans*. Curr Opin
432 Microbiol **9**(6), 595-601.

433 BOUGEN-ZHUKOV, N., LOH, S.Y., LEE, H.K. & LOO, L.H. (2017). Large-scale image-based screening
434 and profiling of cellular phenotypes. Cytometry A **91**(2), 115-125.

435 BRANDUARDI, P., DUJON, B., FELDMANN, H., GAILLARDIN, C. & PORRO, D. (2012). V: Yeast growth
436 and the yeast cell cycle. Molecular and Cell Biology. Feldmann H.(ur.). Weinheim, Wiley-
437 Blackwell, 175-204.

438 CAMPOS, L.M., LEMOS, A.S., SILVA, T.P., OLIVEIRA, L.G., NASCIMENTO, A.L.R., CARVALHO, J.J., DE
439 MORAES, A.C., ROCHA, V.N., AGUIAR, J.A., SCIO, E., APOLÔNIO, A.C., MELO, R.C.N. &
440 FABRI, R. (2019). *Mitracarpus frigidus* is active against S*almonella enterica* species including
441 the biofilm form. Ind Crops Prod **141**, 111793.

442 CAMPOS, L.M., MELO, L., LEMOS, A.S.O., GUEDES, M.C.M.R., SILVA, T.P., FIG.UEIREDO, G.F., REIS
443 JUNIOR, F.B., ROCHA, V.N., MELO, R.C.N., ARAÚJO, M.G.F., APOLONIO, A.C.M., SCIO, E. &
444 FABRE, A. (2018). *Mitracarpus frigidus*: A promising antifungal in the treatment of
445 vulvovaginal candidiasis. Ind Crops Prod **12**, 731-739.

446 DE BARROS, P.P., ROSSONI, R.D., DE SOUZA, C.M., SCORZONI, L., FENLEY, J. & JUNQUEIRA, J. (2020).
447 Candida Biofilms: An Update on Developmental Mechanisms and Therapeutic Challenges.
448 Mycopathologia **185**, 415-420..

449 DEL POZO, J.L. (2018). Biofilm-related disease. Expert Rev Anti Infect Ther **16**(1), 51-65.

450 DOUGLAS, L.J. (2003). Candida biofilms and their role in infection. Trends Microbiol **11**(1), 30-36.

451 FANNING, S. & MITCHELL, A.P. (2012). Fungal biofilms. PLoS Pathog **8**(4), e1002585.

452 FARAHANI, N., PARWANI, A.V. & PANTANOWITZ, L. (2015). Whole slide imaging in pathology:
453 advantages, limitations, and emerging perspectives. Pathol Lab Med Int **7**, 23-33.

454 GHANNOUM, M.A. & RICE, L.B. (1999). Antifungal agents: mode of action, mechanisms of
455 resistance, and correlation of these mechanisms with bacterial resistance. Clin Microbiol Rev
456 **12**(4), 501-517.

457 HAGEAGE, G.J. & HARRINGTON, B.J. (1984). Use of calcofluor white in clinical mycology. Lab Med
458 **15**(2), 109-112.

459 HALL-STOODLEY, L., COSTERTON, J.W. & STOODLEY, P. (2004). Bacterial biofilms: from the natural
460 environment to infectious diseases. Nat Rev Microbiol **2**(2), 95-108.

461 KAPUSCINSKI, J. (1995). DAPI: a DNA-specific fluorescent probe. Biotech Histochem **70**(5), 220-
462 233.

463 KEAN, R., DELANEY, C., RAJENDRAN, R., SHERRY, L., METCALFE, R., THOMAS, R., MCLEAN, W.,
464 WILLIAMS, C. & RAMAGE, G. (2018). Gaining Insights from Candida Biofilm Heterogeneity:
465 One Size Does Not Fit All. J Fungi (Basel) **4**(1).

466 KERNIEN, J.F., SNARR, B.D., SHEPPARD, D.C. & NETT, J.E. (2017). The Interface between Fungal
467 Biofilms and Innate Immunity. Front Immunol **8**, 1968.

468 KURIYAMA, T., WILLIAMS, D.W., BAGG, J., COULTER, W.A., READY, D. & LEWIS, M.A. (2005). In
469 vitro susceptibility of oral Candida to seven antifungal agents. Oral Microbiol Immunol **20**(6),
470 349-353.

471 LAGREE, K., DESAI, J.V., FINKEL, J.S. & LANNI, F. (2018). Microscopy of fungal biofilms. Curr Opin
472 Microbiol **43**, 100-107.

473 LEE, H.N., MAGWENE, P.M. & BREM, R.B. (2011). Natural variation in CDC28 underlies
474 morphological phenotypes in an environmental yeast isolate. Genetics **188**(3), 723-730.

475 LEMOS, A.S., FLORÊNCIO, J.R., PINTO, N.C., CAMPOS, L.M., SILVA, T.P., GRAZUL, R.M., PINTO, P.F.,
476 TAVARES, G.D., SCIO, E. & APOLÔNIO, A.C.M. (2020). Antifungal activity of the natural
477 coumarin scopoletin against planktonic cells and biofilms from a multidrug-resistant *Candida*
478 *tropicalis* strain. Front Microbiol **11**, 1525.

479 LEMOS, A.S.O., CAMPOS, L.M., MELO, L., GUEDES, M., OLIVEIRA, L.G., SILVA, T.P., MELO, R.C.N.,
480 ROCHA, V.N., AGUIAR, J.A.K., APOLONIO, A.C.M., SCIO, E. & FABRI, R.L. (2018).
481 Antibacterial and Antibiofilm Activities of Psychorubrin, a Pyranonaphthoquinone Isolated
482 From *Mitracarpus frigidus (Rubiaceae*). Front Microbiol **9**, 724.

483 LIU, Y., AUBREY, W., MARTIN, K., SPARKES, A., LU, C. & KING, R.D. (2011). The analysis of yeast
484 cell morphology features in exponential and stationary Phase. J Biol Syst **19**(04), 561-575.

485 MALM, A., CHUDZIK, B., PIERSIAK, T. & GAWRON, A. (2010). Glass surface as potential in vitro
486 substratum for Candida famata biofilm. Annals of Agricultural and Environmental Medicine
487 **17**(1), 115-118.

488 MELO, R.C.N., RAAS, M.W.D., PALAZZI, C., NEVES, V.H., MALTA, K.K. & SILVA, T.P. (2019). Whole
489 Slide Imaging and Its Applications to Histopathological Studies of Liver Disorders. Front
490 Med (Lausanne) **6**, 310.

491 NOBILE, C.J. & JOHNSON, A.D. (2015). *Candida albicans* Biofilms and Human Disease. Annu Rev
492 Microbiol **69**, 71-92.

493 PAIVA, L.C., VIDIGAL, P.G., DONATTI, L., SVIDZINSKI, T.I. & CONSOLARO, M.E. (2012). Assessment
494 of in vitro biofilm formation by Candida species isolates from vulvovaginal candidiasis and
495 ultrastructural characteristics. Micron **43**(2-3), 497-502.

496 PAULITSCH, A.H., WILLINGER, B., ZSALATZ, B., STABENTHEINER, E., MARTH, E. & BUZINA, W.
497 (2009). In-vivo Candida biofilms in scanning electron microscopy. Med Mycol **47**(7), 690-
498 696.

499 PFALLER, M.A., DIEKEMA, D.J. & SHEEHAN, D.J. (2006). Interpretive breakpoints for fluconazole and
500 Candida revisited: a blueprint for the future of antifungal susceptibility testing. Clin
501 Microbiol Rev **19**(2), 435-447.

502 RAMAGE, G., RAJENDRAN, R., SHERRY, L. & WILLIAMS, C. (2012). Fungal biofilm resistance. Int J
503 Microbiol **2012**, 528521.

504 RAMAGE, G., VANDEWALLE, K., WICKES, B.L. & LOPEZ-RIBOT, J.L. (2001). Characteristics of biofilm
505 formation by *Candida albicans*. Rev Iberoam Micol **18**(4), 163-170.

506 REX, J.H. (2008). *Reference method for broth dilution antifungal susceptibility testing of filamentous*
507 *fungi: approved standard*. Clinical and Laboratory Standards Institute.

508 ROILIDES, E. & RAMAGE, G. Current perspectives in fungal biofilms. In *MYCOSES*, pp. 13-14.
509 WILEY 111 RIVER ST, HOBOKEN 07030-5774, NJ USA.

510 SACO, A., BOMBI, J.A., GARCIA, A., RAMIREZ, J. & ORDI, J. (2016). Current Status of Whole-Slide
511 Imaging in Education. Pathobiology, **83**(2-3), 79-88.

512 SILVA-DIAS, A., MIRANDA, I.M., BRANCO, J., COBRADO, L., MONTEIRO-SOARES, M., PINA-VAZ, C. &
513 RODRIGUES, A.G. (2015). In vitro antifungal activity and in vivo antibiofilm activity of
514 cerium nitrate against Candida species. J Antimicrob Chemother **70**(4), 1083-1093.

515 SONG, D., LIU, H., JI, H. & LEI, Y. (2019). Whole Slide Imaging for High-Throughput Sensing
516 Antibiotic Resistance at Single-Bacterium Level and Its Application to Rapid Antibiotic
517 Susceptibility Testing. Molecules **24**(13), 2441.

518 UPPULURI, P., CHATURVEDI, A.K., SRINIVASAN, A., BANERJEE, M., RAMASUBRAMANIAM, A.K.,
519 KOHLER, J.R., KADOSH, D. & LOPEZ-RIBOT, J.L. (2010). Dispersion as an important step in
520 the *Candida albicans* biofilm developmental cycle. PLoS Pathog **6**(3), e1000828.

521 WANG, L. & LIN, X. (2012). Morphogenesis in fungal pathogenicity: shape, size, and surface. PLoS
522 Pathog **8**(12), e1003027.

523 WEBSTER, J.D. & DUNSTAN, R.W. (2014). Whole-slide imaging and automated image analysis:
524 considerations and opportunities in the practice of pathology. Vet Pathol **51**(1), 211-223.

525 WIMPENNY, J., MANZ, W. & SZEWZYK, U. (2000). Heterogeneity in biofilms. FEMS Microbiol Rev
526 **24**(5), 661-671.

527 XIE, Z., THOMPSON, A., SOBUE, T., KASHLEVA, H., XU, H., VASILAKOS, J. & DONGARI-BAGTZOGLOU,
528 A. (2012). Candida albicans biofilms do not trigger reactive oxygen species and evade
529 neutrophil killing. J Infect Dis **206**(12), 1936-1945.

530

531

532

533

534

535

536

537 **Figure Legends**

538

539

540

541

542

543 **Supporting information**

544 **Figure S1- Relationship between biofilm area acquired by different scan modalities and**
545 **staining methods.** DAPI and Calcofluor White (CW)-stained coverslips from three biofilm-forming
546 *Candida* species (*C. albicans* ATCC 10231*, C. glabrata* ATCC 2001*,* and *C. tropicalis* ATCC 750)
547 were digitally scanned in two different modalities (fluorescence and bright-field). Regression
548 analyses between covered-biofilm area were statistically significant ($P<0.0001$) when methods were
549 compared: (A) Brigh-tfield *versus* Fluorescence - DAPI, (B) Bright-field *versus* Fluorescence - CW
550 and (C) Fluorescence - DAPI *versus* Fluorescence - CW.

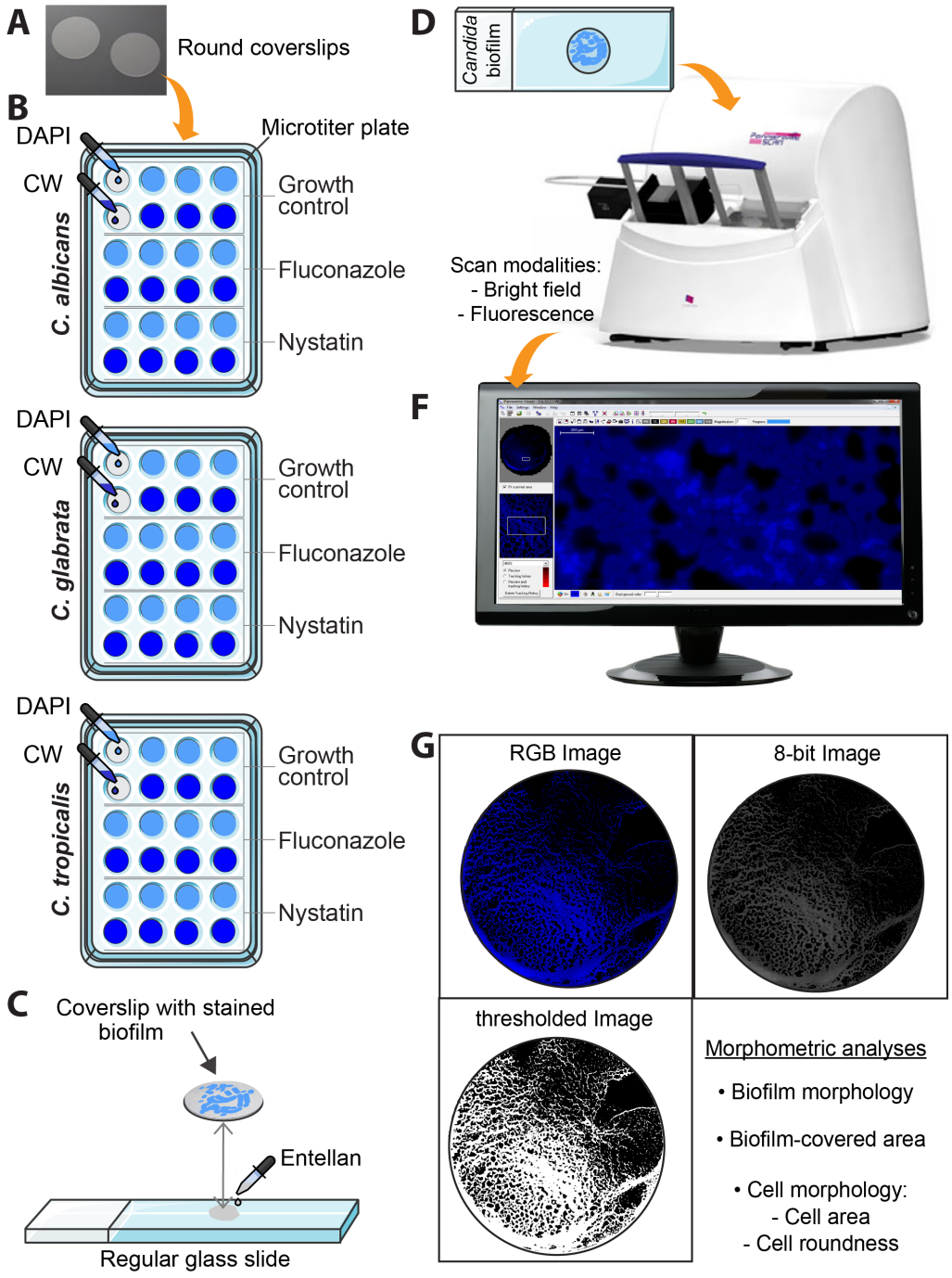

Figure 1 - Assessment of biofilms with WSI. (A) Round glass coverslips were used for growing biofilms in cultures. (B) Cultures of *C. albicans*, *C. glabrata* and *C. tropicalis* were cultivated in microtiter plates with or without the presence of antifungals agents and developed biofilms on the surface of coverslips were stained with two different fluorophores [DAPI and Calcofluor-white (CW); n=4/group/each staining]. (C) Stained coverslips were affixed on regular glass slides using Entellan mounting medium. (D) Glass slides with coverslips were scanned in a digital scanner (3D HistechKft, Budapest, Hungary) in two different modalities (bright-field and fluorescence). (E) High-*resolution images were acquired using Pannoramic Viewer 1.15.2 SP2 RTM software (3D Histechkft* Budapest, Hungary). (F) Virtual images (RGB) were converted to 8-bit (black and white) and thresholded for morphometric analyses using FIJI software.

562

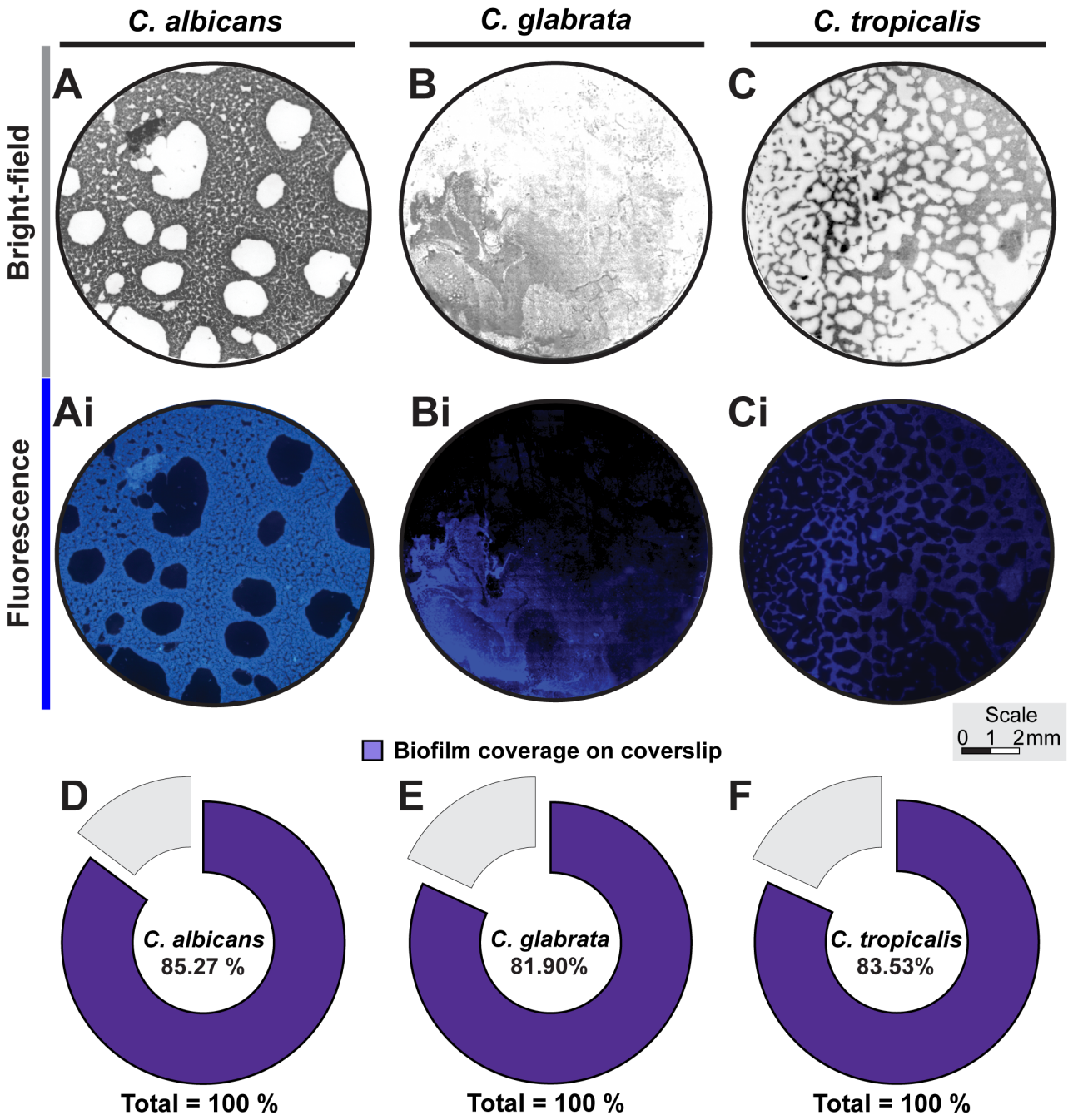

563

564 **Figure 2 - Evaluation of *Candida* biofilms growth with WSI.** Representative virtual images of *C.*
565 *albicans* (A and Ai), *C. glabrata* (B and Bi) and *C. tropicalis* (C and Ci) biofilms growing at the
566 surface of coverslips in the control group acquired under bright-field and fluorescence microscopy. In
567 (D-F), the proportion of biofilm-covered area is shown considering all scan modes. A total of 96
568 high-resolution virtual images covering the total biofilm area were acquired for subsequent viewing
569 and morphometric analyses using FIJI software. Each virtual image represents an entire glass
570 coverslip/slide. Fluorescent images show biofilms stained with DAPI.

571

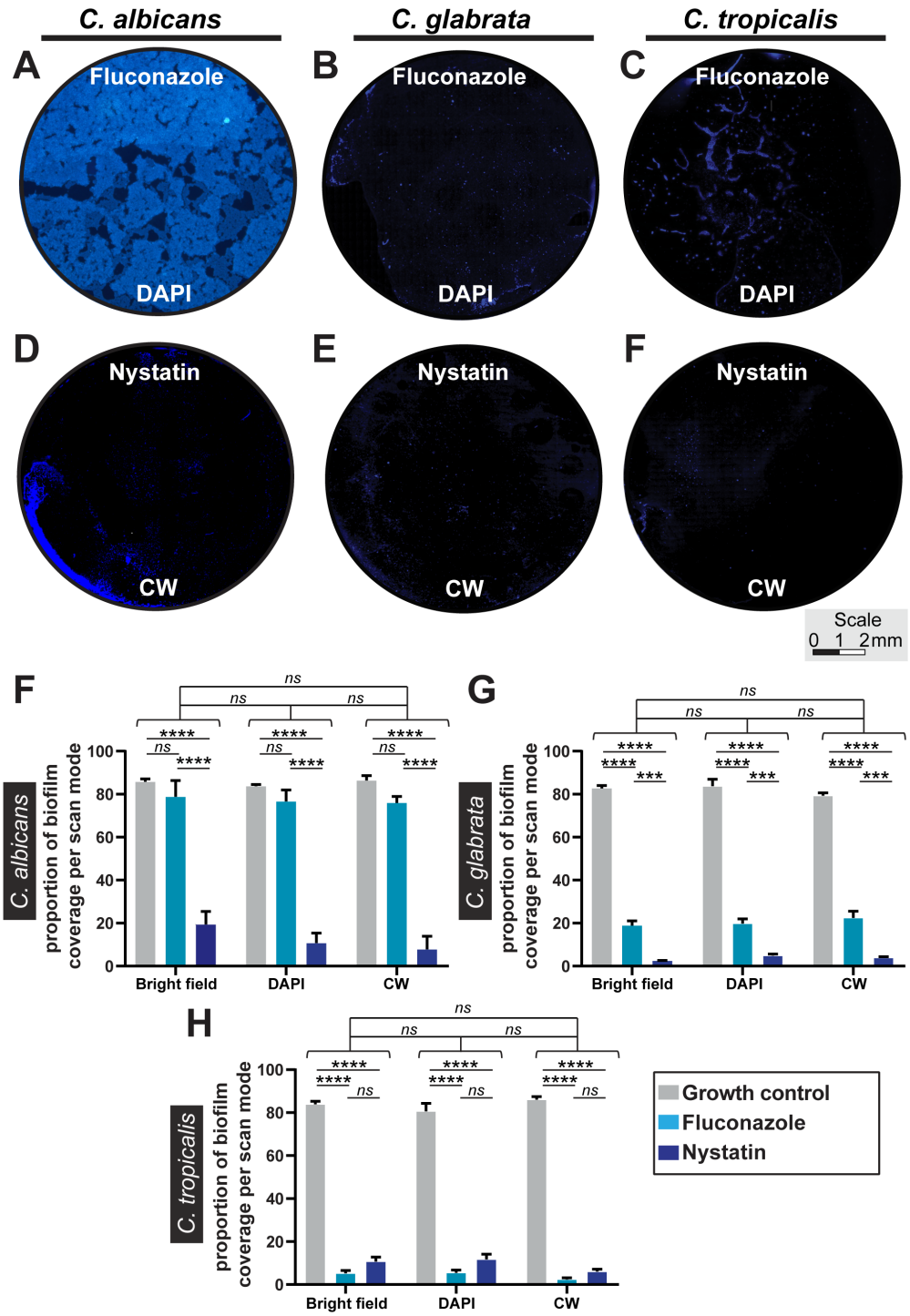

Figure 3 – Evaluation of *Candida biofilms* formation after fluconazole or nystatin treatments. (A-I) Virtual images of biofilms growing at the surface of coverslips in the control group (A-C) and after antifungal treatments (D-I) acquired with different scans strategies. In (J), the biofilm-covered areas were quantitated for each group considering all scan modes. (K) The proportion of biofilm coverage is shown per each scan mode. Significant (asterisks, $P<0.0001$) and non-significant (NS) differences are indicated when groups were compared.

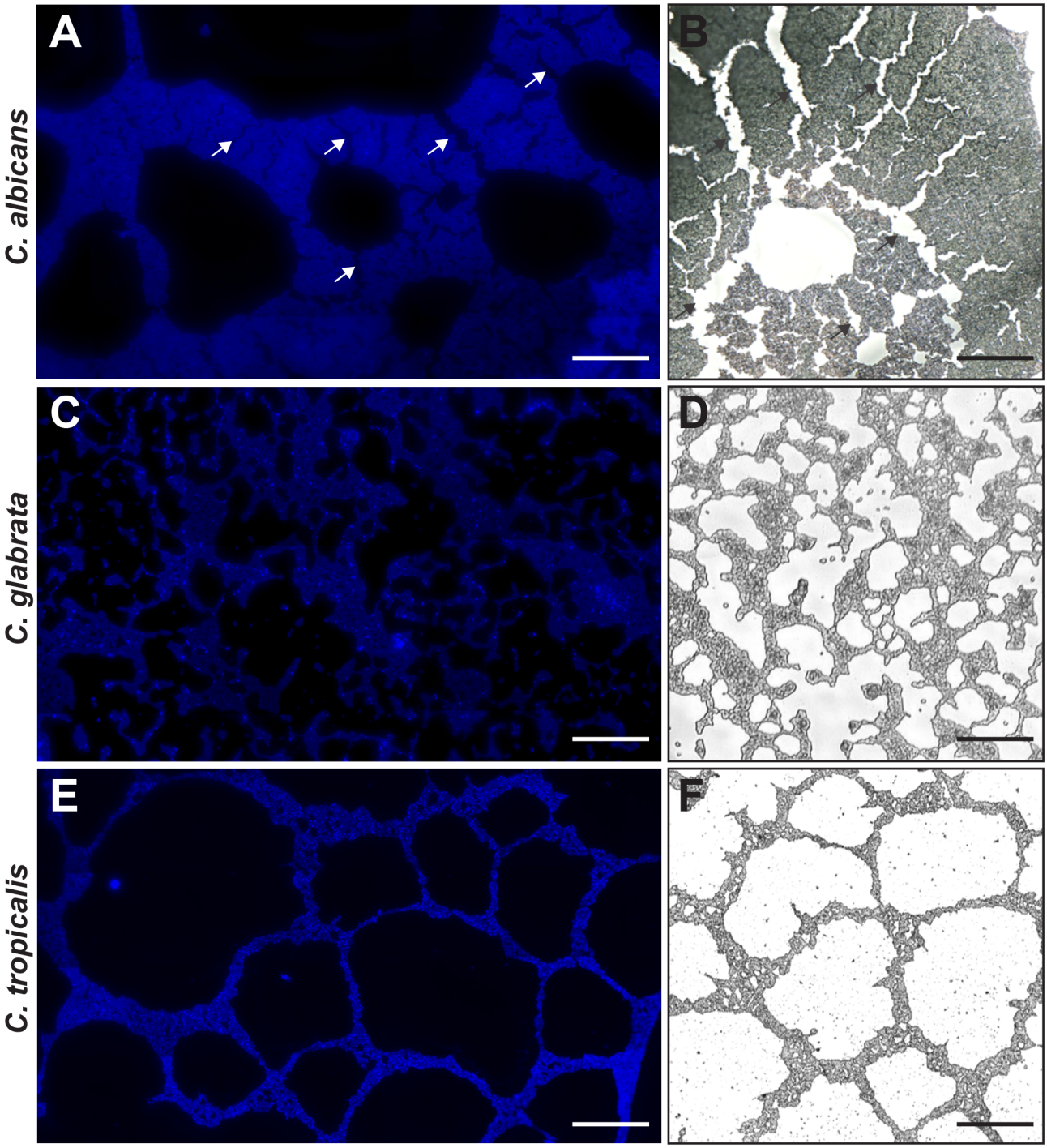

Figure 4 - Architecture of *Candida* biofilms normally growing in cultures. (A, B) *C. albicans* form a highly dense biofilm with channel-like structures (arrows) flowing through the biofilm extent. (C, D) *C. glabrata* biofilm is characterized by a meshwork shape with thin filamentous stretches of relatively small fungal cells surrounding an empty, almost round opening. (E, F) *C. tropicalis* biofilm shows a honeycomb-like chambers. WSI images were acquired under bright-field (A, C, F) or fluorescence/DAPI staining (B, D, F) modes. Scale bar, 200 µm.

587

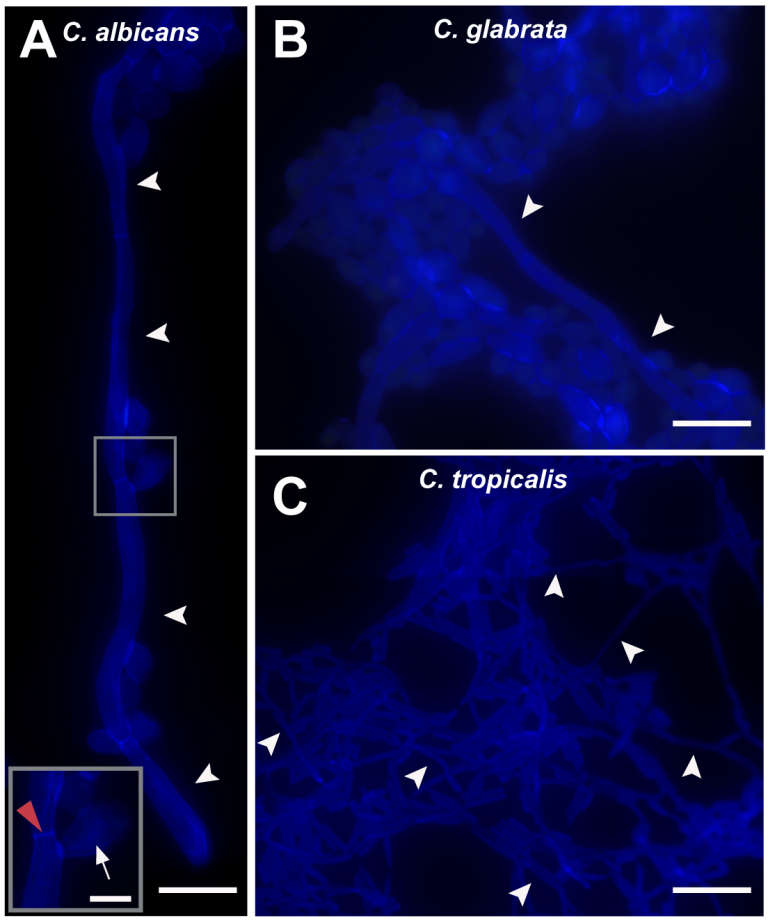

588

589

590 **Figure 5 - Hyphal forms with typical morphology (arrowheads) are seen in *C. albicans* (A), *C.***
591 ***glabrata* (B) and *C. tropicalis* (C) biofilms.** In (A), the presence of constriction septa separating
592 filamentous cells is indicated by a red arrowhead in higher magnification in the inset. Budding cells
593 (arrow) are also noted. Scale bar, 15 µm.

594

595

596

597

598

599

600

601

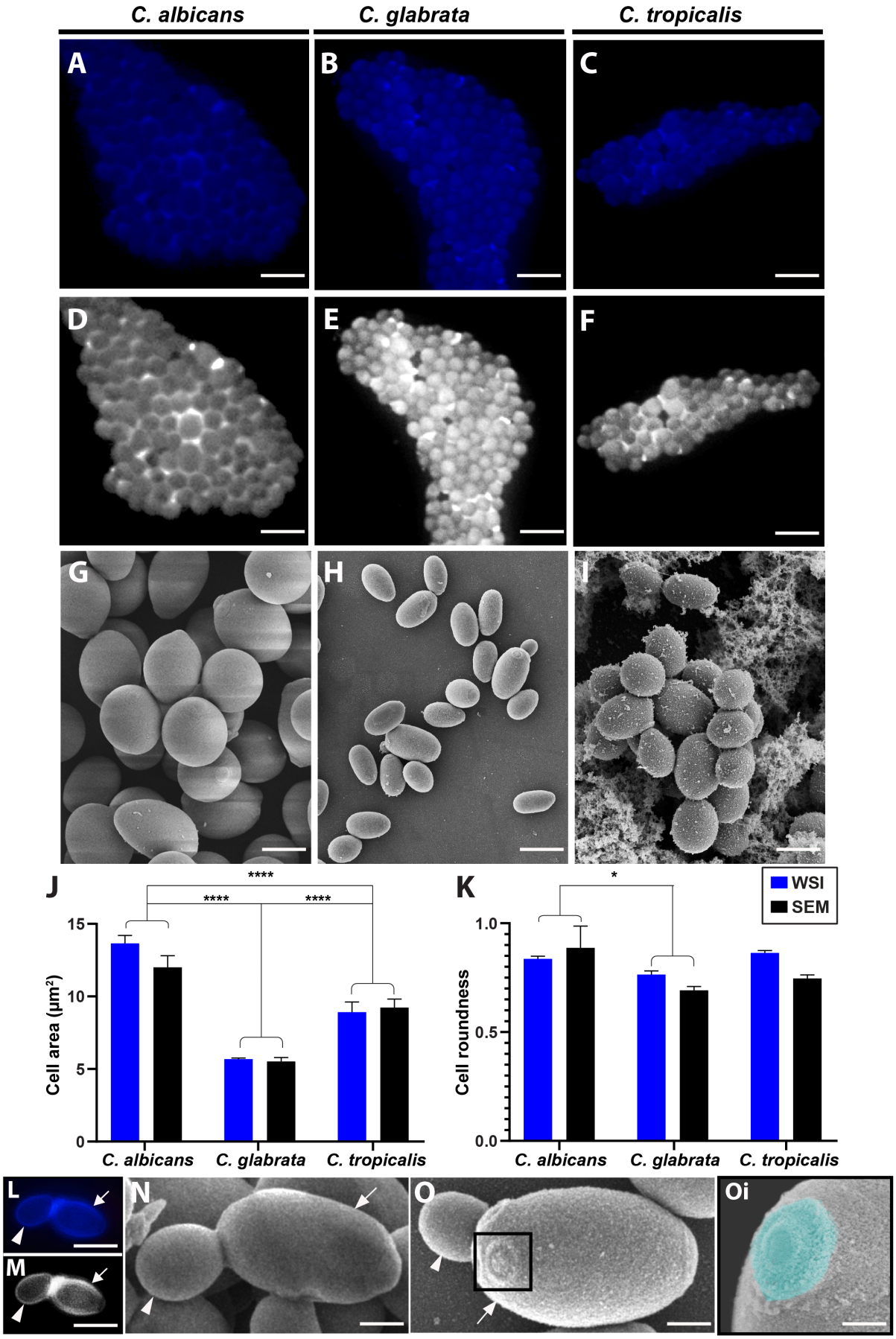
C. albicans
C. glabrata
C. tropicalis
A
B
C
D
E
F
G
H
I
J
****
****
****
Cell area (µm²)
15
10
5
0
C. albicans
C. glabrata
C. tropicalis
K
*
WSI
SEM
Cell roundness
1.0
0.5
0.0
C. albicans
C. glabrata
C. tropicalis
L
M
N
O
Oi

602

603 **Figure 6 – Single-cell morphology of *Candida* biofilms normally growing in cultures.** (A-C)
604 High-resolution WSI images of *C. albicans, C. glabrata* and *C. tropicalis*, respectively, observed at
605 bright-field mode. In (D-F), the same fields are observed by WSI in fluorescence mode. In (G-I),
606 images from scanning electron microscopy (SEM) shows the same shapes observed by WSI. Note in
607 (I) that part of the fungal extracellular matrix is observed in the background. (J) Cell area and (K) cell
608 roundness were quantitated in images acquired with WSI and SEM, with no difference between these
609 two tools. In (L-O) observe by WSI (L and M) or SEM (N-O) the presence of budding cells
610 (arrowheads) originated from mother yeast cells (arrows). Note in (Oi) a bud scar (highlighted in
611 cyan) on the surface of a yeast cell. A total of 332 WSI images and 348 electron micrographs were
612 analysed. Asterisk indicates significant difference ($P = 0.01$). Scale bar; 6 µm (A-F), 3 µm (G-I), 4
613 µm (L-M), 800 nm (N, O), 400 nm (Oi). Asterisk indicates significant difference (J: $P < 0.0001$;
614 K: $P = 0.01$).
615
616
617
618
619
620
621
622
623

Whole slide imaging to understand Candida biofilm growth and response to antifungals

Maximilian W. D. Raas, Thiago P. Silva, Jhamine C. O. Freitas, Lara M. Campos, Rodrigo L. Fabri, Rossana C.N. Melo

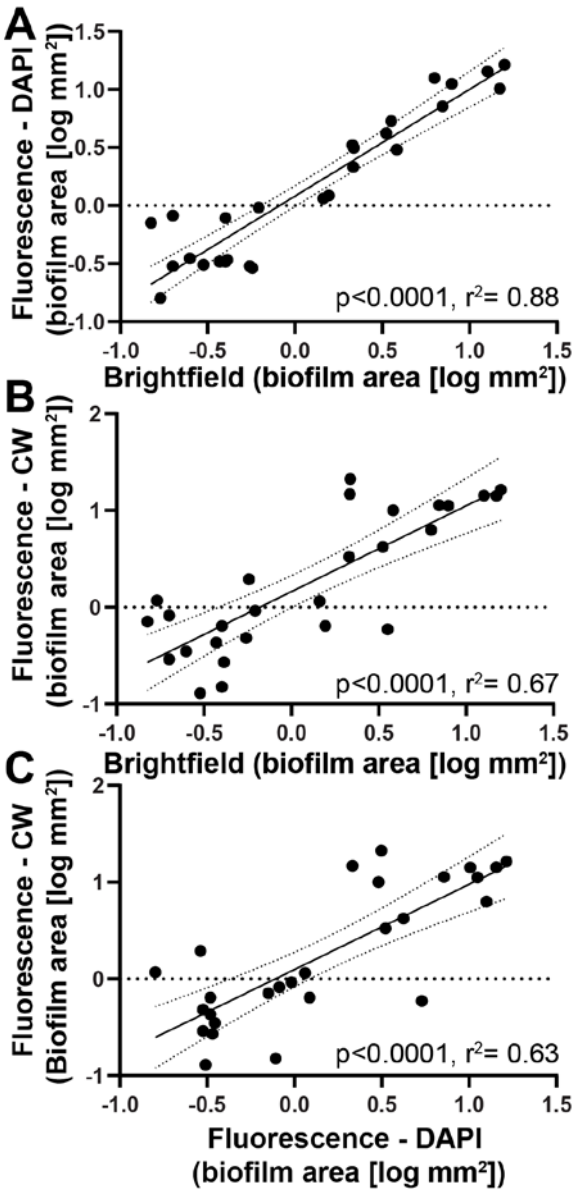

S1 Fig- Relationship between biofilm area acquired by different scan modalities and staining. DAPI and CW stained coverslips from the three Candida species were digitally scanned in two different modalities (fluorescence and bright field). Regression analyses between covered-biofilm area were statistically significant (p> 0.0001) when methods were compared: (A) Brightfield *versus* Flurescence - DAPI, (B) Brightfield *versus* Flurescence - CW and (C) Flurescence - DAPI *versus* Flurescence - CW.